

Evaluation of the LiTransit Kernel for BRDF Modeling

Feng Gao (1,2), Xiaowen Li (1,3), Alan Strahler (1), Crystal Schaaf (1)

(1) Dept. of Geography and Center for Remote Sensing, Boston Univ., 725 Commonwealth Ave.,

Boston, MA 02215, USA, Tel. (617) 353-8033, Fax. (617) 353-3200, email: fgao@crsa.bu.edu

(2) Nanjing Institute of Geography and Limnology, Chinese Academy of Science, China

(3) College of Resource and Environment, Beijing Normal Univ., China

ABSTRACT

Kernel-driven bidirectional reflectance distribution function (BRDF) models are widely used in the description of BRDF properties of land types. To further improve the ability of kernel-driven semiempirical models to capture the BRDF of the surface, a geometrical kernel, the LiTransit kernel, has recently been derived. The LiTransit kernel strives to improve the physical parameterization of geometric-optical effects while keeping the ability to fit the data well and to calculate accurate albedos. It is part of our continuing work on the enhancement of semiempirical kernel-driven BRDF models. We tested the new kernel's performance using ground, airborne and spaceborne bidirectional measurements obtained from various sources. The results show that the LiTransit kernel retains the ability to fit BRDF shapes in sparsely vegetated regions as well as the LiSparse-Reciprocal kernel while providing continuity in the transition from sparse to dense vegetation covers.

We have also tested the new kernel combination RossThick/LiTransit to ascertain its capacity to predict bidirectional reflectance and directional hemispherical reflectance (black-sky albedo) when

presented with data with a MODIS-like sampling. The new kernel combination performs better in modeling reflectance at high view zenith angles, particularly under high illumination zenith angles than the Li-Sparse-Reciprocal kernel which is currently in operational use. The bihemispherical reflectance (white-sky albedo) derived using spaceborne POLDER (Polarization and Directionality of the Earth's Radiation instrument) samples with the RossThick-LiSparse-Reciprocal and the RossThick-LiTransit models are very similar. Their correlation coefficient is larger than 0.99. This demonstrates that the RossThick-LiTransit model retains the best features of RossThick-LiSparse-Reciprocal model while incorporating more realistic physics into the formulation. An analysis of the noise sensitivity of the RossThick-LiTransit model shows that the noise propagation factors of both the RossThick-LiSparse-Reciprocal and RossThick-LiTransit models are smaller than 50 percent for data with MODIS like sampling when the number of looks vary from 7 to 16.

1. INTRODUCTION

The operational MODIS (MODerate Resolution Imaging Spectroradiometer) BRDF/Albedo product uses registered, multiband, multirate, atmospherically corrected surface reflectance data from the MODIS and MISR (Multiangle Imaging SpectroRadiometer) instruments to best fit a bidirectional reflectance distribution function (BRDF) in seven spectral bands at a 1 km resolution on a 16-day cycle (Strahler et al., 1994; Wanner et al., 1997; Lucht et al., 2000). It provides bihemispherical reflectance, directional hemispherical reflectance and nadir BRDF-adjusted reflectances (NBAR) which are of interest to the global climate modeling and remote sensing communities. Directional hemispherical reflectance (or black-sky albedo – BSA) is defined as the integral of the BRDF over the view hemisphere for a given illumination angle. It is a function of solar zenith angle (Wanner et al., 1997). Bihemispherical reflectance (or white-sky albedo – WSA) is defined as the double integral of the BRDF over the viewing and illumination hemispheres. It is a constant describing total reflectance under isotropic illumination

(Wanner et al., 1997). White-sky albedo may be deemed an approximation to completely overcast skies, while black-sky albedo represents direct beam clear skies without diffuse skylight. Both of these cases are the extreme cases and are defined as surface properties and do not depend on the atmospheric state. The actual spectral albedo is approximated by their linear combination weighted by the proportions of diffuse and direct skylight approximate to the atmospheric condition (Lewis et al., 1994).

In the MODIS at-launch BRDF/Albedo algorithm, a linear kernel-based semiempirical model, the reciprocal RossThick-LiSparse model, is used. This algorithm has been widely validated with regard to its model fitting ability, its performance under sparse angular sampling and its sensitivity to noise. Its retrievals have been found to be generally reliable (Hu et al., 1997; Privette et al., 1997; Lucht et al., 2000). One possible defect in the LiSparse-Reciprocal kernel is that the value of LiSparse-Reciprocal kernel approaches infinity as the view zenith angle approaches 90 degrees. This does not usually impact the resultant albedo computation of the operational product since the contribution of these angles (which is weighted by sine-cosine product of the view zenith angle) is very small in the numerical integration required. But in order to further improve the extrapolation ability of the RossThick-LiSparse-Reciprocal model, a alternative geometrical kernel, LiTransit, has recently been derived (Li et al., 1999). It uses the LiSparse kernel under conditions of smaller solar and view zenith angles and then transitions to the LiDense kernel smoothly at larger solar and view zenith angles. The LiTransit kernel strives to improve the physical parameterization of geometric-optical effects while retaining the data-fitting abilities of both the LiSparse and LiDense kernels. This paper compares the capacity of the RossThick-LiTransit model to fit data, to predict reflectances and to handle noisy data with that of the RossThick-LiSparse-Reciprocal model and with the other commonly used semiempirical Rahman-Pinty-Verstraete (RPV) model (Rahman et al., 1993).

2. THE LiTransit KERNEL

A linear kernel-driven BRDF model can be expressed as:

$$BRDF = f_{iso} + f_{vol} * k_{vol}(\theta_i, \theta_v, \phi) + f_{geo} * k_{geo}(\theta_i, \theta_v, \phi) \quad (1)$$

where k_{vol} , a function of view zenith θ_v and illumination zenith θ_i and relative azimuth ϕ , describes the volume scattering from canopy and k_{geo} , a similar function describes the surface scattering from canopy. These functions are called volumetric and geometric kernels, respectively. In Eq. (1), f_{vol} and f_{geo} are the weights for the volumetric and geometric kernels, respectively, and f_{iso} is a constant corresponding to isotropic reflectance. In the first derivation of our kernel-driven BRDF models, each volumetric and geometric kernel was actually a series of kernels selected according the vegetation cover (Roujean et al., 1992; Strahler et al., 1995; Wanner et al., 1995). A suitable expression for the volumetric kernel was first derived by Roujean et al. (1992) from the radiative transfer formulation of Ross (1981). It is termed the RossThick kernel, as it assumes a dense leaf canopy. Li (in Strahler et al., 1994) then provided the RossThin kernel for the case of small leaf area index (LAI). In the first derivation of the geometrical kernel, the Li series of kernels were derived by Li (in Strahler et al., 1995) from the geometric-optical BRDF model for forest canopies by Li and Strahler (1986, 1992). The Li series of kernels can be grouped into two categories. The first of these are approximations for a "sparse" canopy of discrete objects and the second is for approximations of a "dense" spacing of objects. They are denoted as LiSparse kernels and LiDense kernels, respectively.

Kernel-driven BRDF models were derived to try to retain some of the physical meaning of BRDF models while providing an approximation useful in a linear equation. They are thus semiempirical BRDF models. Since they are linear models, they can be inverted analytically. Both the Terra-MODIS BRDF/Albedo and the ADEOS-POLDER BRDF products utilized kernel-driven BRDF models. In the at-launch MODIS BRDF/Albedo algorithm, the reciprocal RossThick-LiSparse model was used. In the ADEOS-POLDER BRDF product, the Roujean BRDF model (Roujean et al., 1992) was used.

The LiTransit kernel is a recently derived enhanced geometrical kernel (Li et al., 1999a). Since both the Roujean BRDF model and at-launch MODIS BRDF/Albedo algorithm use the RossThick

volumetric kernel and validations reveal that the RossThick kernel is better suited to description of BRDF than RossThin kernel (Hu et al., 1997; Privette et al., 1997), we also use the RossThick kernel as the volumetric component and use it to compose a new kernel-driven linear BRDF model called RossThick-LiTransit model (Li et al., 1999a).

The Ross kernels are expressed in a reciprocal form in which an exchange of illumination and view angle gives a similar result. The Li kernels were first published in a nonreciprocal form (Wanner et al., 1995) and then changed to reciprocal form (Lucht, 1998; Lucht et al., 2000). The current operational MODIS BRDF/Albedo algorithm uses the reciprocal form of LiSparse kernel and thus the model is called the RossThick-LiSparse-Reciprocal model. However, the LiTransit kernel is not reciprocal. Li et al. (1999a, 1999b) point out that the principal of reciprocity does not generally apply at the scale of the remote sensing pixel if there is nonsymmetrical crosstalk in the remotely sensed pixel and therefore the LiTransit is a nonreciprocal kernel. The LiTransit kernel is derived from the nonreciprocal LiSparse and LiDense kernels. The nonreciprocal LiSparse kernel can be written as

$$K_{LiSparse} = A(\theta_i, \theta_v, \phi) - B(\theta_i, \theta_v, \phi) \quad (2)$$

where

$$A(\theta_i, \theta_v, \phi) = \frac{1}{2}(1 + \cos \xi') * \sec(\theta_v') \quad (3)$$

$$B(\theta_i, \theta_v, \phi) = \sec(\theta_i') + \sec(\theta_v') - O(\theta_i, \theta_v, \phi) \quad (4)$$

and

$$O = \frac{1}{\pi}(t - \sin t \cos t)(\sec \theta_i' + \sec \theta_v') \quad (5)$$

$$\cos t = \frac{h \sqrt{D^2 + (\tan \theta_i' \tan \theta_v' \sin \phi)^2}}{b \sec \theta_i' + \sec \theta_v'} \quad (6)$$

$$D = \sqrt{\tan^2 \theta_i' + \tan^2 \theta_v' - 2 \tan \theta_i' \tan \theta_v' \cos \phi} \quad (7)$$

$$\cos \xi' = \cos \theta_i' \cos \theta_v' + \sin \theta_i' \sin \theta_v' \cos \phi \quad (8)$$

$$\theta' = \tan^{-1} \left(\frac{b}{r} \tan \theta \right) \quad (9)$$

The crowns are assumed to be spheroids with vertical length $2b$, horizontal width $2r$, and distance h to their center above the ground. In the LiTransit kernel, we use $b/r=1$ and $h/b=2$, which are the same values used in the operational MODIS BRDF/albedo algorithm. Using the same terms, the nonreciprocal LiDense kernel can be expressed as

$$K_{LiDense} = 2 * A(\theta_i, \theta_v, \phi) / B(\theta_i, \theta_v, \phi) - 2 = 2 * K_{LiSparse} / B(\theta_i, \theta_v, \phi) \quad (10)$$

Therefore, when we reach the boundary where

$$B(\theta_i, \theta_v, \phi) = 2 \quad (11)$$

we have:

$$K_{LiDense} = K_{LiSparse}$$

This captures the transition that should occur whenever the area proportion of this clumping plus the shadow approaches unity and the LiDense kernel should replace LiSparse kernel (which was designed for the sparsely located clumps and associated shadows). The LiTransit kernel is defined as (Li et al., 1999)

$$K_{LiTransit} = \begin{cases} K_{LiSparse} & \text{if } B(\theta_i, \theta_v, \phi) \leq 2 \\ K_{LiDense} & \text{if } B(\theta_i, \theta_v, \phi) > 2 \end{cases} \quad (12)$$

From Eq. (4), we know $B(\theta_i, \theta_v, \phi)$ depends on the illumination and view geometries. When $B(\theta_i, \theta_v, \phi)$ is less than and equal to 2, the LiTransit kernel uses the LiSparse formulation. When $B(\theta_i, \theta_v, \phi)$ is larger than 2, the LiTransit kernel uses the LiDense formulation. Figure 1(a) shows the boundaries of $B(\theta_i, \theta_v, \phi) = 2$ at different solar zenith angles. As the solar zenith angle increases, the boundary of $B(\theta_i, \theta_v, \phi) = 2$ shrinks and the proportion of Li-Dense kernel in Li-Transit kernel increases. When solar zenith angle increases to 60 degrees, the boundary of $B(\theta_i, \theta_v, \phi) = 2$ diminishes to a point and the

LiTransit kernel is then equal to the LiDense kernel. Figure 1(b) shows the contours of the Li-Transit kernel in hemisphere space for a 40 degrees solar zenith angle. Within the boundary of $B(\theta_i, \theta_v, \phi) = 2$, the LiSparse kernel is used. Beyond that boundary, the LiDense kernel is used. The figure shows that the LiTransit kernel moves very smoothly across that boundary from the Li-Sparse kernel to the Li-Dense kernel.

Figure 1

3. DATA DESCRIPTION AND INVERSION METHODS

Seventy-five BRDF measurements, accumulated from many different sources, were used in this study. Most of them are from PARABOLA radiometer measurements (Deering et al., 1986). Kimes' radiometer measurements (Kimes et al., 1983; 1986) and airborne POLDER data (Leroy et al., 1996) are also included in the collection.

Seven land cover types measured by the PARABOLA radiometer were chosen for testing the capacity of the model to predict reflectance and albedo and to assess its sensitivity to noisy data. The canopy LAI values, the ranges of solar zenith angles and the white-sky albedos calculated from the original measurements are listed in table 1.

Table 1

According to Privette et al. (1997) and Deering et al. (1992a;b, 1994), the lava soil field site is located in the vicinity of Lunar Crater Volcanic Field approximately 250 km northwest of Las Vegas, Nevada. This site was one of several established for the Geologic Remote Sensing Field Experiment (GRSFE) in 1989. The site was located on an intermediate-aged lava flow that had been partly buried by aeolian silt and fine sand. It contained a sparse cover of grasses and low growing woody plants. The grassland sites were measured during the First ISLSCP Field Experiment (FIFE) of 1987. The sites were burned in the spring of the previous year to remove litter. The cotton sites were located in the Maricopa Agricultural Research Center south of Phoenix, Arizona, and were measured on September 1991. The

cotton was a uniform row-planted canopy with approximately 90 percent ground coverage and the soil was dry. The three boreal forest sites (old aspen, jack pine, and the black spruce) were measured in Central Saskatchewan, Canada, in 1994. These sites were located at Boreal Ecosystem-Atmosphere Study (BOREAS) tower/tram sites in the southern study area of the experiment. The old aspen site was located in Prince Albert National Park and contained mostly mature quaking aspen. The understory was a dense growth of hazelnut shrubs with some wild rose, and the ground cover was about 50 percent leaf litter with a variety of herbs and grasses. The canopy closure including the hazelnut understory averaged 89 percent. The black spruce site tree cover was mainly composed of the black spruce. The understory was young black spruce. The average canopy closure was about 55 percent. The jack pine sites had a pure stand of jack pine forest. Tree height ranged from 11 to 14 meters and the average canopy closure was estimated to be about 61 percent, and the sandy soil was very well drained. In this study, only red (650-670nm) and near infrared (810-840nm) wavebands were used.

Airborne POLDER measurements in the area of La Crau, France during June 1991 (Leroy et al., 1996) were also used to extract BRDF information. The site is covered by a wide variety of vegetation types, such as sunflower, corn, vines, grass, vegetables and sorghum. After registration of several POLDER images, data with various view and illumination angles were obtained for the red (630-670 nm) and near-infrared (830-870 nm) wavebands (Hu et al., 1997).

Spaceborne POLDER/ADEOS BRDF data were also used on the tests. This data set is provided for 16 IGBP landcover classes, which include evergreen needleleaf forest, evergreen broadleaf forest, deciduous needleleaf forest, deciduous broadleaf forest, mixed forests, closed shrublands, open shrublands, woody savannas, savannas, grasslands, permanent wetlands, croplands, urban and built-up, cropland/natural vegetation mosaic, snow and ice, and barren or sparsely vegetated. The data were obtained during two periods of two months each (November and December 1996, May and June 1997). The choice of two periods allowed us to observe the temporal changes of the BRDF. An individual BRDF

data set was comprised of POLDER level 2 surface reflectance data for a given 6 km resolution pixel, at 443 nm, 670 nm, and 865nm, with associated sun and view zenith angles and relative azimuth between view and sun directions. Although correction accounting for molecular scattering correction was applied, the correction for tropospheric aerosols was not taken into account for these data set (Bicheron et al., 1999). The POLDER/ADEOS samples include measurements from small solar zenith angles (4.7 degrees) to large solar zenith angles (67.8 degrees).

The BRDF field measurements by Kimes were also used in the validation. They include measurement of plowed field, corn field, orchard grass and grass lawn with 0, 25, 50, and 97 percent of vegetation cover measured near Beltsville, Maryland (Kimes, 1983) and annual grassland, hard wheat, steppe grass, irrigated wheat, and soybean with 4, 11, 5, 70, and 90 percent of vegetation cover measured in Northern Africa (Kimes et al., 1985). Data collected in the red (580-680 nm) and the near-infrared (730-1100 nm) bands were used in the test.

These extensive data sets were used with three models in this comparison. The models are (1) the reciprocal RossThick-LiSparse model; (2) the nonreciprocal RossThick-LiTransit model; and (3) the four-parameter Rahman-Pinty-Verstraete (RPV) model (Rahman et al., 1993; Engelsen et al., 1996). Because the RPV model is a nonlinear BRDF model, a nonlinear Powell algorithm was used for the parameter inversion. The parameters relate to the amplitude of the BRDF, the value of the hot spot parameter, and the value of the variable for the Minnaert function were constrained between 0.0 and 1.0. The value of the asymmetry factor in the Heney-Greenstein function was constrained between -1.0 and 1.0.

We also used parameter constraints in the inversion of the reciprocal RossThick-LiSparse model and nonreciprocal RossThick-LiTransit model. Appropriate ranges of the three parameters were obtained from a priori knowledge of the inversions of the 75 data sets. We calculated the minimum and maximum weights for each kernel and set the weight for the isotropic kernel from 0 to 0.8. The weight for the

volume kernel ranged from 0 to 0.6 and the weight for the surface kernel ranged from 0 to 0.3. Note that only a lower boundary constraint was used, i.e., if the retrieved parameter was negative, it was reset to 0.

4. CAPACITY TO FIT DATA

One of the important factors in evaluating a BRDF model is its capacity to fit data. In this test, all 75 ground and airborne measurements were inverted and their root mean square errors (RMSE) were drawn with 2-D scattering graphics. Figure 2 is the RMSE results of the 75 data sets in both the red and NIR wavebands. Figure 3 is the RMSE results of the POLDER/ADEOS data in the red and NIR wavebands. Both figures show that there is no obvious difference in the ability of the three models to fit these BRDF data sets. However, all models show that they have the smallest RMSE in dealing with the spaceborne measurements. This may imply that due to the 7 km spatial resolution and the stronger blurring of atmosphere, spaceborne POLDER data contain less detailed information and thus are more appropriate for 3-4 parameter semiempirical models than more detailed field and airborne measurements.

Figure 2

Figure 3

5. CAPACITY TO PREDICT REFLECTANCE AND ALBEDO

Sampling over the viewing or illumination hemisphere is usually limited for current spaceborne platforms. The Terra-MISR instrument provides nine viewing angle observations simultaneously with the same solar zenith angle. The ADEOS-POLDER provides more observations but is still limited in terms of solar zenith angle. Even when accumulating data over several days, the variations of solar zenith angle represented in these spaceborne BRDF measurements are still very small. Since albedo is the integral of the BRDF over the view and illumination hemispheres, it is important for a BRDF model to be able to predict reflectance at viewing or illumination angles other than those actually measured. In order to test

the capacity of the BRDF models to predict bidirectional reflectance and directional-hemispherical reflectance (black-sky albedo), we selected several data sets with MODIS-like sampling from the PARABOLA measurements of seven land covers mentioned above.

The data with MODIS-like sampling were chosen from the measurements which have the most similar geometry to that of the MODIS-AM observations. The operational MODIS BRDF/Albedo algorithm uses 16 days of observations as inputs to retrieve the BRDF. We developed a scheme to find 16 days worth of observations with MODIS-like sampling from the PARABOLA radiometer measurements. First an orbital simulation software called Xsatview (Barnsley et al., 1994) was used to create MODIS observation geometries for the whole globe for all 365 days of the year. Then a deliberately designed searching process was applied to find the observations with the most similar geometries to MODIS observations from the PARABOLA radiometer measurements. Given the limitation of the viewing and solar geometries of PARABOLA radiometer measurements, the simulated MODIS-like sampling is just the best approximation to the real MODIS-Terra measurements. Figure 4 shows the variation of solar zenith angles (SZN) in MODIS data sets to a fixed single solar zenith angle in PARABOLA radiometer measurements. It shows the differences of solar zenith angles between MODIS-like observation in this paper and real MODIS observations. From the figure, we can see the variation of solar zenith angle at the smaller SZN is bigger than at larger SZN. Therefore it is more difficult to find a corresponding MODIS-like data from PARABOLA radiometer measurements for the smaller SZN observations. However, the variation of solar zenith angles of MODIS-like observations and of MODIS observations within 20 to 70 degrees is very small. Therefore, to ensure a good approximation of MODIS-like data, we did not include the data with SZNs smaller than 20 or larger than 70 in these tests.

Figure 4

These MODIS-like data serve as simulated MODIS-Terra observations during 16 days at a certain geo-location and certain date of the year. In other studies, Privette et al. (1997) simulated MODIS

observations by defining four view azimuth angle sectors to restrict sampling of MODIS-like data. These are not strictly MODIS-like observations. Lucht (1998) used Myneni's 3D BRDF forward model (Myneni et al., 1992) and Xsatview to create MODIS-like data sets. However this has the defect of comparing a model to a model (Myneni's 3D BRDF model to linear semiempirical kernel-driven BRDF models). The simulated MODIS-like data in this paper used real measurements with MODIS-like geometries. Figure 5 compares the two sets of geometries of MODIS-like observations and of MODIS observations with solar zenith angles at 35 and 60 degrees respectively. It shows the differences in the viewing geometries of MODIS-like observations and MODIS observations. The MODIS-like observations at higher solar zenith angles are better captured than those at lower solar zenith angles due to the geometries of PARABOLA radiometer measurements.

Figure 5

Once these sets of 16 continuous days of observations were selected for the seven land covers, each of them was then randomly subset to create a series of realistic data sets. These subset data sets consist of MODIS-like data with the number of looks varying from 7 to 16 (in operational MODIS BRDF/Albedo algorithm, analytical inversion of kernel-driven BRDF model was done only when there are at least 7 observations during 16 days observations). For each number of looks, five of these subset data sets were randomly created. Therefore, for each of the land cover types at each solar zenith angle, we have $5 \text{ (subset)} * 9 \text{ (7-15 looks)} + 1 \text{ (16 looks)} = 46$ data sets to use.

The analytical inversion results of the subset data sets are then compared to the results from the data set as a whole. Table 2 lists the percentage relative differences of black-sky albedo derived by the whole data set and by the MODIS-like data set in the red and NIR band for the seven different land cover types. They are the average values of the 46 subset data sets. Except for soil, which is a difficult case for all three of the models to fit, the average percentage differences derived by the whole data set and the MODIS-like data set are less than 10 percent for the red waveband and less than 6 percent for the NIR

waveband. Therefore the models' abilities to calculate black-sky albedo at the same solar zenith angle are very similar.

Table 2

Figure 6 is a scatter plot of white-sky albedo as derived by the RossThick-LiSparse-Reciprocal model and the RossThick-LiTransit model with spaceborne POLDER data. The results show that the white-sky albedos from the two models are very consistent. The correlation coefficients of white-sky albedo of two methods are 0.998 in red band and 0.990 in NIR band.

Figure 6

In the prediction of directional reflectance at very high view zenith angles, the RossThick-LiTransit model works more reliably than the RossThick-LiSparse-Reciprocal model. Figure 7 shows the bidirectional reflectance in the principal solar plane. In order to show the measured reflectance on the principal plane, the solar zenith angles associated with the field data for the land cover types are used in the figure 7. The bidirectional reflectances are calculated from the inversion results of the whole data set. From the figure, we can see both of models have the good abilities to fit the measurements (Note only those observations in the principal plane are drawn). The overall abilities to fit measurements have been discussed in the section 4. Although we haven't actual PARABOLA observations at very high view zenith angles, the more realistic results of RossThick-LiTransit on the prediction of the directional reflectance at the very high view zenith angles are obvious. The bi-directional reflectances from the RossThick-LiSparse-Reciprocal model can even become negative when view zenith angles exceed 85 degrees (dotted line), an effect caused by the increasingly large value of the reciprocal LiSparse kernel when the view zenith angle nears 90 degrees. As noted earlier, however, since the directional reflectances at such high view zenith angles has only a small contribution to the actual albedo, the RossThick-LiSparse-Reciprocal model still works well in the calculation of the albedo as shown in the white-sky albedo of Figure 6. Note

also that the RossThick-LiTransit model has a more obvious “hot spot.” The ability of the RossThick-LiTransit model to capture the “hot spot” still needs to be investigated in the future.

Figure 7

6. NOISE SENSITIVITY

Noise in BRDF measurements will propagate to the white-sky albedo and the black-sky albedo through BRDF models. However, BRDF models can also serve to filter noise if they capture the true underlying shape of the BRDF well. For linear BRDF models, the noise sensitivity of albedo can be calculated from formula (13) (Gao et al., 1998)

$$SD_{albedo} = \sqrt{W * [G' C_d^{-1} G]^{-1} * W'} \quad (13)$$

where SD_{albedo} is the standard deviation of the retrieved albedo; W is the integral matrix of kernels over observation hemisphere (black-sky) and incident hemisphere (white-sky), G is the kernel matrix of all observations, and C_d is the covariance matrix of the measurements (uncertainties).

Table 3 lists the standard deviations of white-sky albedo and black-sky albedo for two different BRDF models at different latitudes from 60 degrees south to 80 degrees north. The results are produced solely from the MODIS-Terra geometries that were created by Xsatview. In the calculation of the standard deviation of albedo, the standard deviation (uncertainties) of all of the BRDF measurements were assumed equal to 1.0 and the covariances between different observations were set to 0 assuming that different observations may vary freely. The results listed in the table are the average standard deviation of white-sky albedo for 7 to 15 looks that were randomly selected from the geometries of 16 days of continuous observations from the MODIS-Terra geometries. In the table, both the RossThick-LiSparse-Reciprocal model and the RossThick-LiTransit model show a low sensitivity to noise. The mean noise sensitivities for white-sky albedo and black-sky albedo are less than 0.50. That means that more than half

of the noise from the measurements can be filtered out in the black-sky and white-sky albedo products when 7 to 16 MODIS-AM looks are available.

Table 3

7. CONCLUSION

Within the past decade, the importance of the nature of the anisotropic surface reflectance of land cover has been widely recognized. Multiangular remote sensing is not just a research topic but also has operational applications. One of the most successful applications of multiangular remote sensing is the retrieval of land surface albedo. A number of BRDF models have been developed for this purpose. For example, the RossThick-LiSparse-Reciprocal was selected to produce the at-launch BRDF/albedo product from MODIS measurements (Lucht et al., 2000). The Roujean model was used to produce BRDF products for POLDER (Roujean et al., 1992; Leroy et al., 1997). The MISR BRDF/Albedo product will be based on a modified version of the Rahman-Pinty-Verstraete (RPV) model (Rahman et al., 1993; Martonchik, 1997). The purpose of this paper is to introduce the new RossThick-LiTransit model, which was recently derived by Li et al (1999b) to better extrapolate reflectance at very high solar and view zenith angles. It is compared with results from the RossThick-LiSparse-Reciprocal model and the RPV model. These comprehensive comparison shows that the RossThick-LiTransit model, RossThick-LiSparse-Reciprocal model have a similar sum square of errors for 75 field data sets and 395 spaceborne POLDER samples. Therefore they all have a similar ability to fit data well. The Rahman-Pinty-Verstraete model, which uses four parameters in this study to describe the BRDF shape, also does quite well. All three BRDF models are able to calculate black-sky albedo accurately at similar solar zenith angles that correspond to the measurements. The RossThick-LiSparse-Reciprocal model and the RossThick-LiTransit model also produced similar results for white-sky albedo using spaceborne POLDER measurements. However, in the case of observations at very high solar or view zenith angles, the RossThick-LiTransit

model produces more reasonable bidirectional reflectances. Both the RossThick-LiTransit model and the RossThick-LiSparse-Reciprocal models show a low sensitivity to noise in the calculation of white-sky or black-sky albedo.

Further validation of the RossThick-LiTransit model, particularly in its ability to extrapolate to unobserved sun and view angles, will be carried out in the future when more BRDF measurements with multiple solar zenith angles are available from MODIS.

Acknowledgments

This work was supported by NASA contract NAS-5-31369 as part of the MODIS project. We would like to thank Drs. Deering, Bicheron, Leroy, Kimes, and Prof. Xiang for providing BRDF measurements and Dr. Pinty for providing the RPV scientific codes. Thanks are also due to Dr. Nicholas Strugnell for providing reformatted BRDF data.

REFERENCES

Barnsley, M. J., Strahler, A. H., Morris, K. P., and Muller, J. P. (1994) Sampling the surface bidirectional reflectance distribution function (BRDF): 1. Evaluation of current and future satellite sensors. *Remote Sens. Rev.*, 8:271-311.

Bicheron, P. and Leroy, M. (1999) BRDF signatures of major biomes observed from space, submitted to *J. of Geophys. Res.*

Deering, D. W., and Leone, A. (1986) A sphere-scanning radiometer for rapid directional measurement of sky and ground radiance. *Remote Sens. Environ.*, 19:1-24.

Deering, D. W., Eck, T. F., and Grier, T. (1992a) Shinnery oak bidirectional reflectance properties and canopy model inversion. *IEEE Trans. Geosci. Remote Sens.*, 20:339-348.

Deering, D. W., Middleton, E. M., Irons, J. R., Blad, B. L., Walter-Shea, E. A., Hays, C. J., Walthall, C., Eck, T. F., Ahmad, S. P., and Banerjee, B. P. (1992b) Prairie grassland bidirectional reflectance measured by different instruments at the FIFE site, *J. Geophys. Res.*, 97:18,887-18,903.

Deering, D., W., Middleton, E. M., and Eck, T. F. (1994) Reflectance anisotropy for a spruce-hemlock forest canopy. *Remote Sens. Environ.*, 47:242-260.

Engelsen, O., Pinty, B., Verstraete, M. M. and Martonchik, J.V. (1996) Parametric bidirectional reflectance factor models: Evaluation, improvements and applications. *EC Joint Research Centre, Technical Report*, EUR 16426 EN, 114 pp.

Gao, F., Strahler, A. H., Lucht, W., Xia, Z. and Li, X. (1998) Retrieving albedo in small sample size. *1998 IEEE Int. Geosci. and Remote Sens. Symp. Proc.*, Volume V:2411-2413.

Hu, B., Lucht, W., Li, X., and Strahler, A. H. (1997) Validation of kernel-driven models for the BRDF of land surfaces. *Remote Sens. Environ.*, 62:201-214.

Kimes, D. S. (1983) Dynamics of directional reflectance factor distribution for vegetation canopies. *Appl. Opt.*, 22:1364-1372.

Kimes, D.S., Newcomb, W. W., Nelson, R.F., and Schutt, J.B. (1986) Directional reflectance distributions of hardwood and pine forest canopy. *IEEE Trans. Geosci. Remote Sens.*, 24: 281-293.

Leroy, M. and Breon, F. M. (1996) Surface reflectance angular signatures from airborne POLDER data. *Remote Sens. Environ.*, 57:97-107.

Leroy, M., Deuze, J. L., Breon, F. M., Hautecoeur, O., Herman, M., Buriez, J., Tanre, D., Bouffies, S., Chazette, P., and Roujean, J. L. (1997) Retrieval of atmosphere properties and surface bidirectional reflectance over land from POLDER ADEOS. *J. Geophys. Res.*, 102:17023-17037.

Lewis, P. and Barnsley, M. J. (1994) Influence of the sky radiance distribution on various formulations of the earth surface albedo. In *Proc. Conf. Physics, Measures, and Signals*, Val d'Isere, France, pp. 707-715.

Li, X. and Strahler, A. H. (1986) Geometric-optical bidirectional reflectance modeling of a conifer forest canopy. *IEEE Trans. Geosci. Remote Sens.*, 24: 906-919.

Li, X. and Strahler, A. H. (1992) Geometric-optical bidirectional reflectance modeling of the discrete crown vegetation canopy: Effect of crown shape and mutual shadowing. *IEEE Trans. Geosci. Remote Sens.*, 30: 276-292.

Li, X., Wang, J., and Strahler, A. H. (1999a) Apparent reciprocity failure in BRDF of structured surfaces. *Progress of Natural Science*, 8(4): 456-460.

Li, X., Gao, F., Chen L., and Strahler, A. H. (1999b) Derivation and validation of a new kernel for kernel-driven BRDF models. *Remote Sensing for Earth Science, Ocean and Sea Ice Application, SPIE Proc. Series*, 3868:368-379, Florence, Italy.

Lucht, W. (1998) Expected retrieval accuracies of bidirectional reflectance and albedo from EOS-MODIS and MISR angular sampling. *J. Geophys. Res.*, 103:8763-8778.

Lucht, W. and Lewis, P. (2000) Theoretical noise sensitivity of BRDF and albedo retrieval from the EOS-MODIS and MISR sensors with respect to angular sampling. *Int. J. Remote Sens.*, 21(1): 81-98.

Lucht, W., Schaaf, C. B., and Strahler A. H. (2000) An algorithm for the retrieval of albedo from space using semiempirical BRDF models. *IEEE Trans. Geosci. Remote Sens.*, 38(2): 977-998.

Myneni, R. B., Asrar, G. and Hall, F. G. (1992) A three-dimensional radiative transfer method for optical remote sensing of vegetated land surfaces. *Remote Sens. Environ.*, 41:105-121.

Martonchik, J. V. (1997) Determination of aerosol optical depth and land surface directional reflectances using multi-angle imagery. *J. Geophys. Res.*, 102: 17,015-17,022.

Privette, J.L., Eck, T.F. and Deering, D.W. (1997) Estimating spectral albedo and nadir reflectance through inversion of simple BRDF models with AVHRR/MODIS-like data. *J. Geophys. Res.*, 102(D24): 29,529-29,542.

Rahman, H., Pinty, B. and Verstraete, M. M. (1993) Coupled surface-atmosphere reflectance (CSAR) model. 2. Semiempirical surface model usable with NOAA advanced very high resolution radiometer data. *J. Geophys. Res.*, 98:20,791-20,801.

Ross, J. K. (1981) *The Radiation Regime and Architecture of Plant Stands*, Dr. W. Junk, Norwell, Mass., 392 pp.

Roujean, J. -L., Leroy, M., and Deschamps, P.-Y. (1992) A bidirectional reflectance model of the Earth's surface for the correction of remote sensing data. *J. Geophys. Res.*, 97(D18): 20,455--20,468.

Strahler, A. H., Li, X., Liang, S., Muller, J. -P, Barnsley, M. J. and Lewis P. (1994) MODIS BRDF/Albedo Product: Algorithm Theoretical Basis Document. *NASA EOS-MODIS Doc.*, v2.1, 55 pp.

Strahler, A. H., Barnsley M. J., d'Entremont R., Hu, B., Lewis, P., Li, X., Muller, J. P., Schaaf, C. B., Wanner, W. and Zhang, B. (1995) MODIS BRDF/Albedo Product: Algorithm Theoretical Basis Document. *NASA EOS-MODIS Doc.*, v3.2, 63 pp.

Wanner, W., Li, X., and Strahler, A. H. (1995) On the derivation of kernels and kernel-driven models of bidirectional reflectance. *J. Geo. Res.*, 100(D10): 21077-21089.

Wanner, W., Strahler, A. H., Hu, B., Li, X., Schaaf, C. B., Lewis, P., Muller, J. -P., and Barnsley, M. J. (1997) Global retrieval of bidirectional reflectance and albedo over land from EOS MODIS and MISR data: Theory and algorithm. *J. Geophys. Res.* 102: 17143-17161.

Figure 1. (a) The boundaries of $B(\theta_i, \theta_v, \phi) = 2$ for four different solar zenith angles.

(b) LiTransit kernel value and the circle of $B(\theta_i, \theta_v, \phi) = 2$ (solar zenith angle: 40 degrees).

Radius represents view zenith angle, the azimuth angle represents relative azimuth, with the solar azimuth angle at 0° .

Figure 2. Scatter plots of RMSEs from different models with 75 measurements (ground and airborne) shows that there is no significant difference in data fitting abilities among the three BRDF models.

Figure 3. Same as Figure 2 but using POLDER/ADEOS data (spaceborne). The better fitting of spaceborne POLDER than field and airborne measurements may imply that because of 7 km spatial resolution and stronger blurring of atmosphere, spaceborne POLDER data contain less detailed information and thus are more appropriate for 3-4 parameter semiempirical models than more detailed field and airborne measurements.

Figure 4. Variation of solar zenith angle for 16 continuous days of MODIS observations which have the most similar solar zenith angle to MODIS-like data with a fixed single solar zenith angle.

Figure 5. Viewing Geometries of MODIS-like PARABOLA measurements (dot) and real MODIS-Terra (cross) measurements.

Figure 6. White-sky albedo of spaceborne POLDER samples derived by the RossThick-LiSparse-Reciprocal model and the RossThick-LiTransit model in the red and NIR wavebands. White-sky albedo

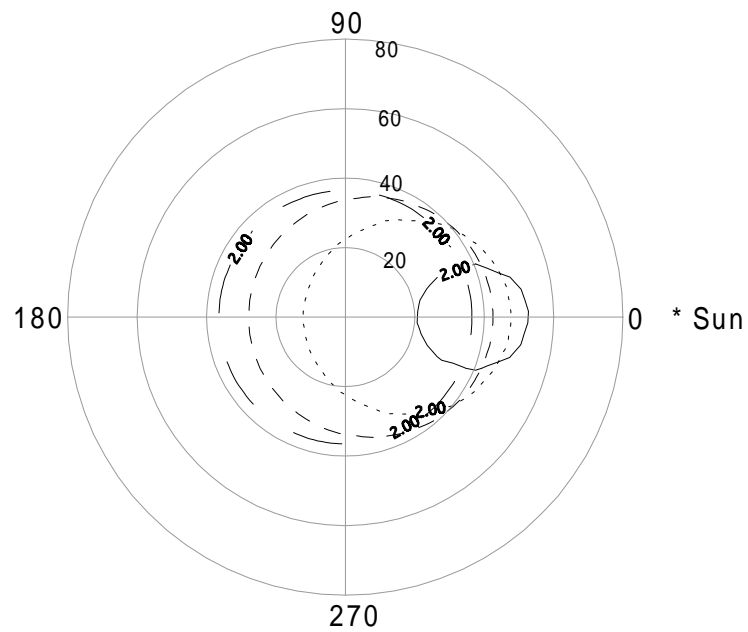
results derived from the two BRDF models are very similar. The correlation coefficients are very high (0.998 for red band and 0.990 for NIR band).

Figure 7. Near-infrared bidirectional reflectance in the principal solar plane for seven different land cover types. Dotted lines, RossThick-LiSparse-Reciprocal model; solid lines, RossThick-LiTransit model; small circles, measurements (Note only those observations in the principal solar plane are displayed). RossThick-LiTransit model gives a more reasonable bidirectional reflectance at very high view zenith angles and shows a more obvious “hot spot.”

Table 1. Test data measured by PARABOLA radiometer.

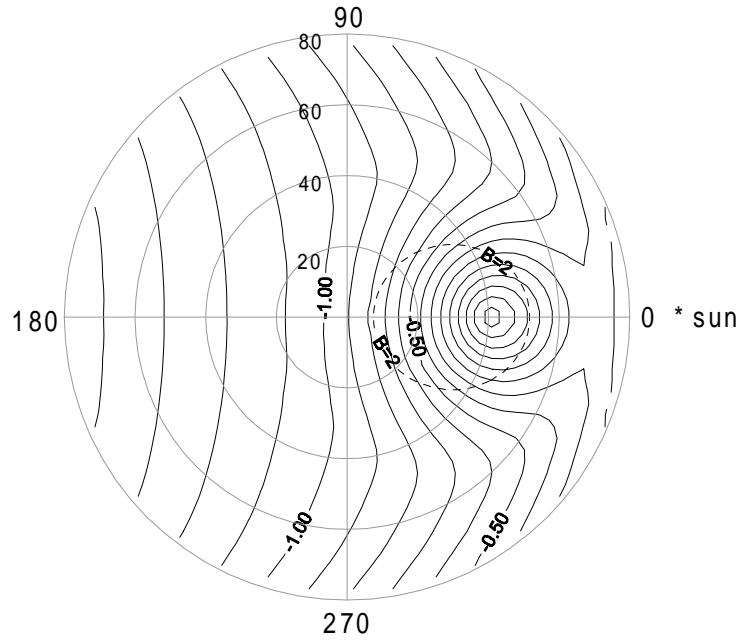
Table 2. Average percentage relative differences of black-sky albedo between the whole data set and MODIS-like data set (7 to 16 looks) with black-sky albedo at same solar zenith angle. LiT, RossThick-LiTransit model; LiS, RossThick-LiSparse-Reciprocal model; RPV, Rahman-Pinty-Verstraete model.

Table 3. Average noise sensitivity of models at different latitude and thus different solar zenith angles. WSA, white-sky albedo; BSA, black-sky albedo.



— SZA=0 - - - - SZA=15 ····· SZA=30
 - - - - SZA=15 ——— SZA=45

(a)



(b)

Figure 1

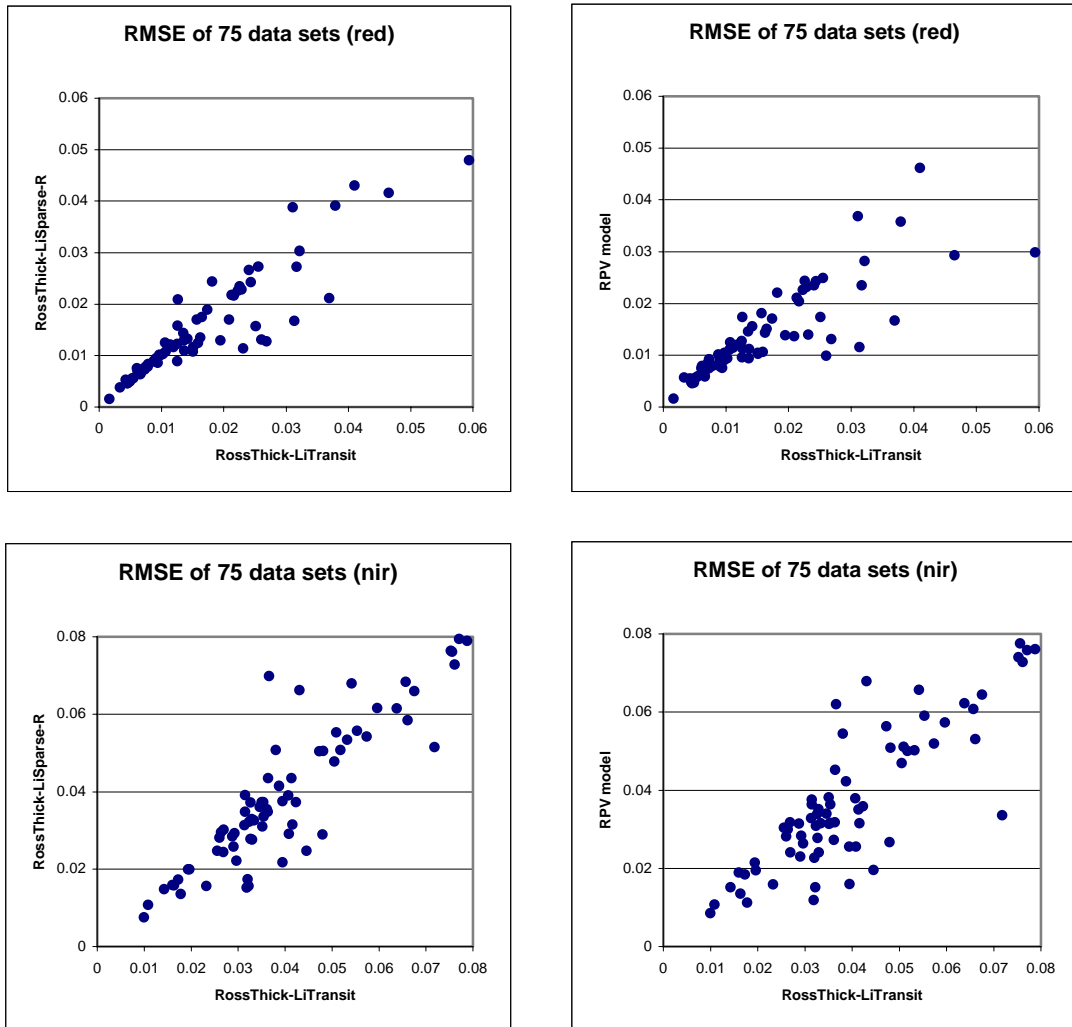


Figure 2

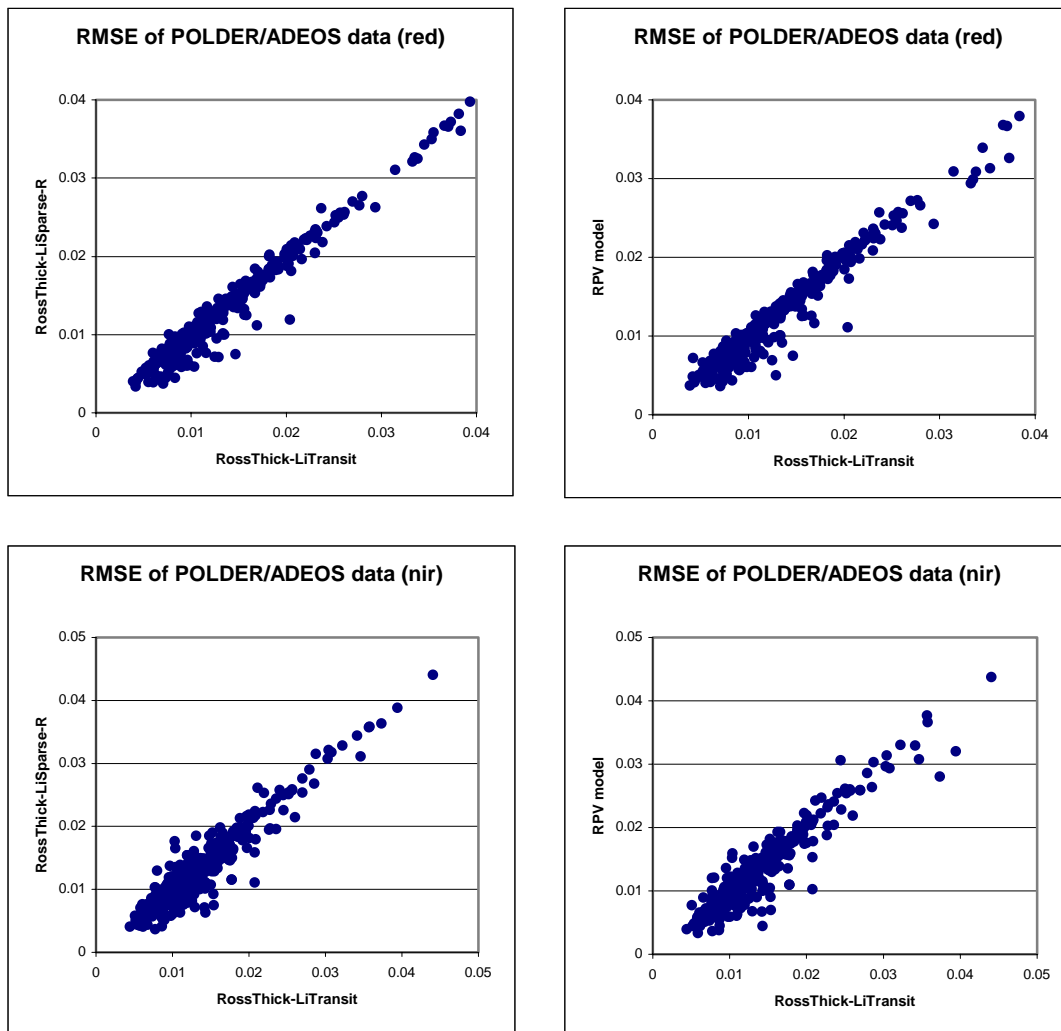


Figure 3

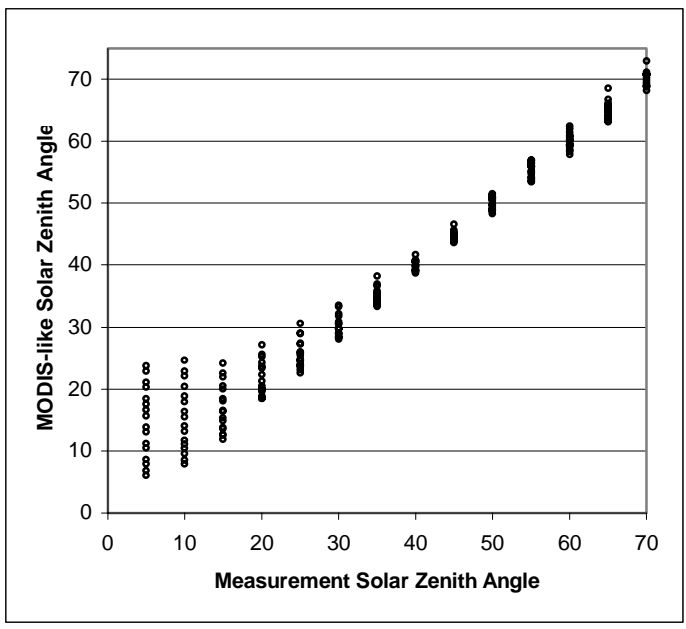


Figure 4

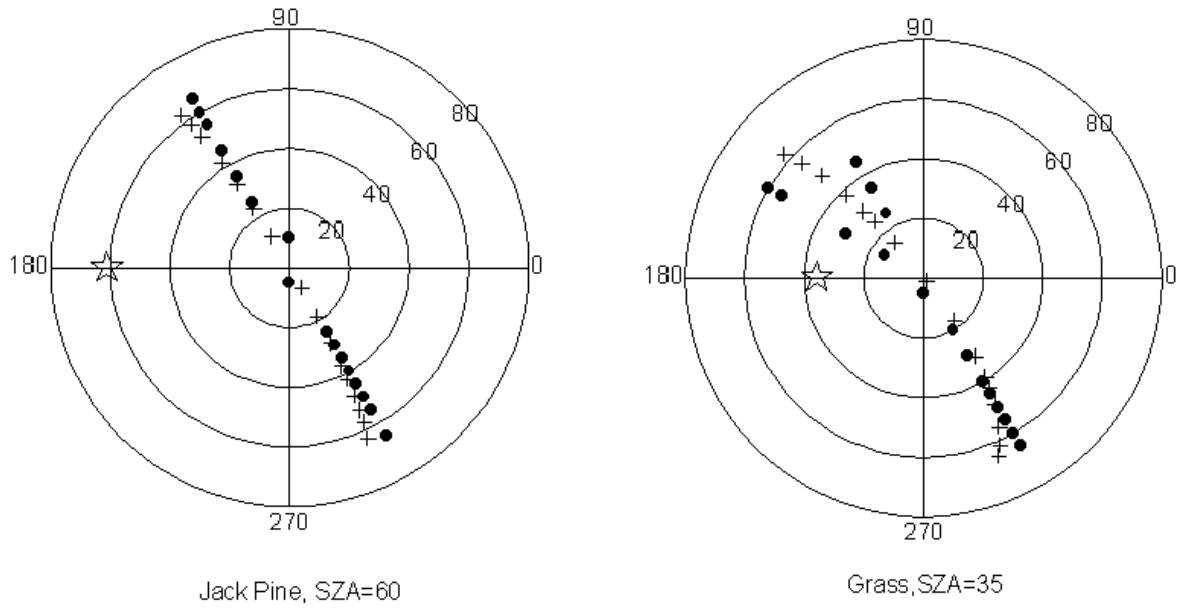


Figure 5

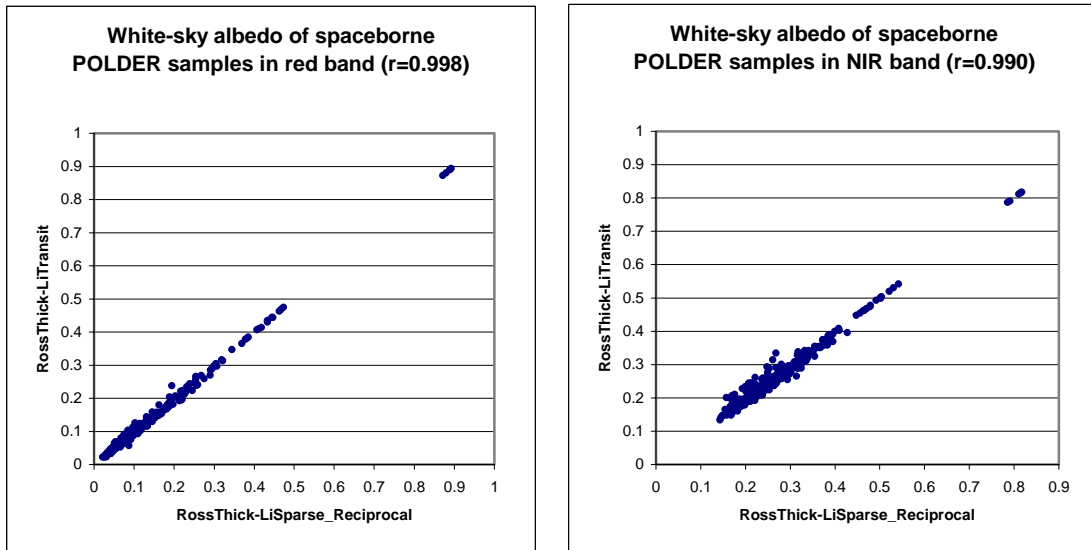


Figure 6

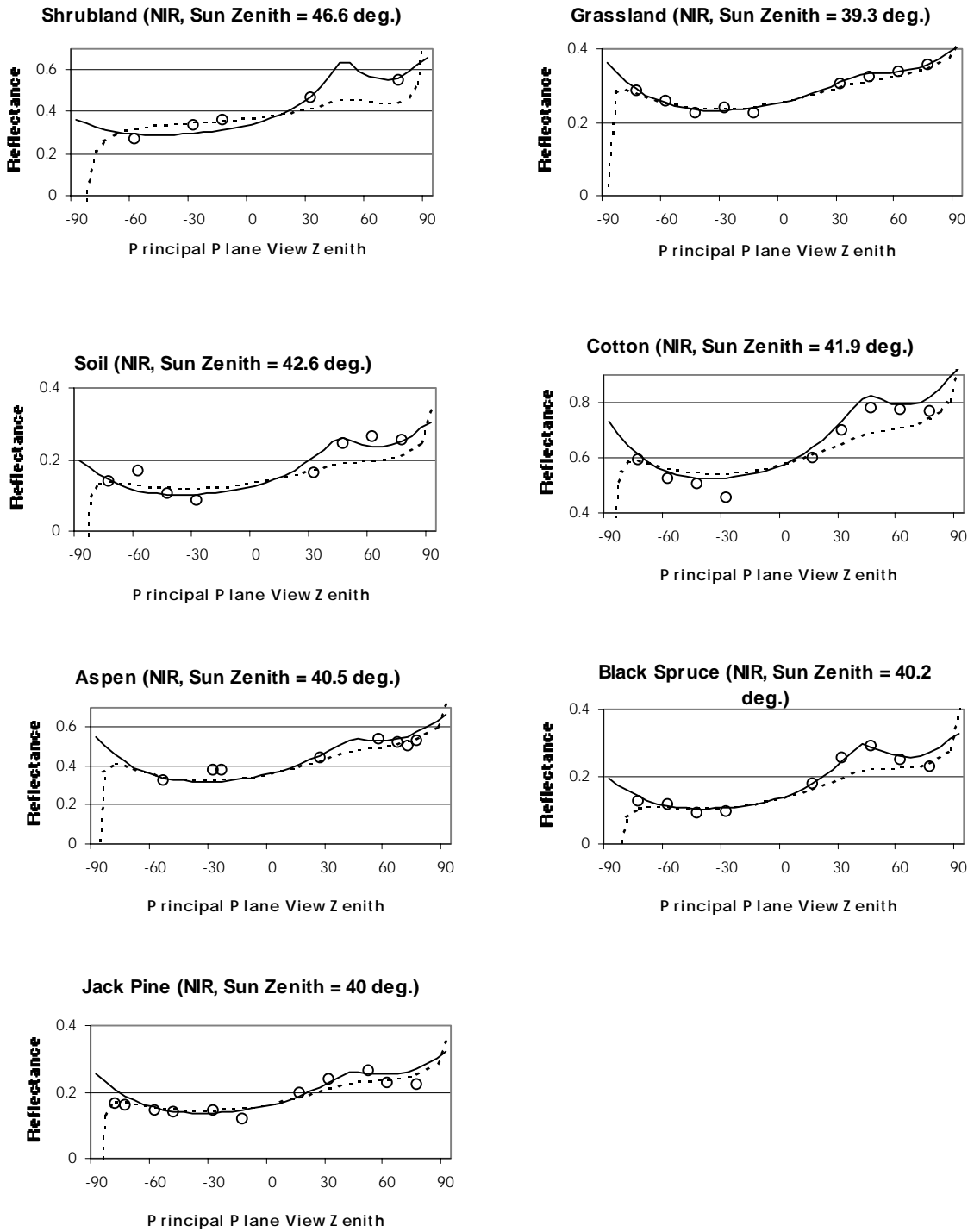


Figure 7

Table 1

Land Cover Type	Number of SZA	SZA Range (degree)	LAI	Red_WSA	NIR_WSA
Soil	6	21-73	<0.1	0.117	0.157
Grass	9	18-68	1.5	0.095	0.289
Shrubland	5	32-77		0.289	0.375
Cotton	7	37-76	4.0	0.035	0.630
Aspen	6	41-65	3.3	0.023	0.422
Black Spruce	8	35-70	6.3	0.030	0.164
Jack Pine	8	15-69	1.2	0.039	0.194

Table 2

Band	Red			Near-Infrared		
	LiT	LiS	RPV	LiT	LiS	RPV
Shrubland	3.712	2.200	2.834	2.613	1.927	2.050
Grass	6.380	6.215	8.001	2.348	2.351	2.774
Soil	9.851	10.493	11.021	9.118	9.312	9.179
Cotton	5.995	6.418	7.998	2.136	1.899	3.114
Aspen	6.530	6.798	5.407	3.618	5.611	6.029
Black Spruce	7.679	8.737	9.502	4.405	3.707	5.299
Jack Pine	4.291	5.660	5.952	2.369	2.555	2.643

Table 3

	RossThick-LiSparse-Reciprocal				RossThick-LiTransit			
	WSA	BSA, 0°	BSA, 30°	BSA, 60°	WSA	BSA, 0°	BSA, 30°	BSA, 60°
60 S	0.3620	0.3881	0.3663	0.3823	0.3488	0.3758	0.3479	0.4011
50 S	0.4190	0.3808	0.3564	0.4809	0.3684	0.3773	0.3468	0.4367
40 S	0.4457	0.3715	0.3431	0.5406	0.3632	0.3685	0.3336	0.4423
30 S	0.3617	0.3608	0.3385	0.4110	0.3509	0.3580	0.3379	0.4103
20 S	0.3782	0.3543	0.3404	0.4250	0.3611	0.3428	0.3336	0.4215
10 S	0.3623	0.3509	0.3390	0.3963	0.3650	0.3364	0.3357	0.4249
0	0.3527	0.3443	0.3368	0.3765	0.3680	0.3382	0.3396	0.4229
10 N	0.3315	0.3345	0.3323	0.3339	0.3637	0.3303	0.3308	0.4166
20 N	0.3392	0.3385	0.3379	0.3411	0.3728	0.3308	0.3318	0.4308
30 N	0.3449	0.3385	0.3395	0.3487	0.3798	0.3336	0.3355	0.4410
40 N	0.3477	0.3413	0.3425	0.3510	0.3755	0.3387	0.3362	0.4339
50 N	0.3633	0.3540	0.3560	0.3679	0.3718	0.3471	0.3389	0.4258
60 N	0.3684	0.3582	0.3604	0.3734	0.3587	0.3602	0.3403	0.4030
70 N	0.3604	0.3356	0.3563	0.3629	0.3399	0.3612	0.3344	0.3752
80 N	0.3503	0.3488	0.3486	0.3510	0.3260	0.3612	0.3309	0.3514
AVE.	0.3658	0.3547	0.3463	0.3895	0.3609	0.3507	0.3369	0.4158